ARTICLES
https://doi.org/10.1038/s41588-019-0413-z
nature genetics

MTHFD1 interaction with BRD4 links folate metabolism to transcriptional regulation

Sara Sdelci[1,13], André F. Rendeiro[1], Philipp Rathert[2,14], Wanhui You[1,3], Jung-Ming G. Lin[1], Anna Ringler[1,3], Gerald Hofstätter[1,3], Herwig P. Moll[4], Bettina Gürtl[1], Matthias Farlik[1], Sandra Schick[1,3], Freya Klepsch[1], Matthew Oldach[1], Pisanu Buphamalai[1], Fiorella Schischlik[1], Peter Májek[1], Katja Parapatics[1], Christian Schmidl[1,15], Michael Schuster[1], Thomas Penz[1], Dennis L. Buckley[5], Otto Hudecz[6], Richard Imre[6], Shuang-Yan Wang[7,8], Hans Michael Maric[7,8], Robert Kralovics[1,9], Keiryn L. Bennett[1], Andre C. Müller[1], Karl Mechtler[2], Jörg Menche[1], James E. Bradner[5], Georg E. Winter[1], Kristaps Klavins[1], Emilio Casanova[4,10], Christoph Bock[1,9,11], Johannes Zuber[2,12] and Stefan Kubicek[1,4]*

The histone acetyl reader bromodomain-containing protein 4 (BRD4) is an important regulator of chromatin structure and transcription, yet factors modulating its activity have remained elusive. Here we describe two complementary screens for genetic and physical interactors of BRD4, which converge on the folate pathway enzyme MTHFD1 (methylenetetrahydrofolate dehydrogenase, cyclohydrolase and formyltetrahydrofolate synthetase 1). We show that a fraction of MTHFD1 resides in the nucleus, where it is recruited to distinct genomic loci by direct interaction with BRD4. Inhibition of either BRD4 or MTHFD1 results in similar changes in nuclear metabolite composition and gene expression; pharmacological inhibitors of the two pathways synergize to impair cancer cell viability in vitro and in vivo. Our finding that MTHFD1 and other metabolic enzymes are chromatin associated suggests a direct role for nuclear metabolism in the control of gene expression.

BRD4 is an important chromatin regulator with roles in gene regulation, DNA damage, cell proliferation and cancer progression[1–4]. The protein is recruited to distinct genomic loci by the interaction of its tandem bromodomains with acetylated lysines on histones and other nuclear proteins[5]. There, BRD4 acts as a transcriptional activator by positive transcription elongation factor (P-TEFb)-mediated stimulation of transcriptional elongation[6]. The activating function of BRD4 on key driver oncogenes like *MYC* have made this epigenetic enzyme an important therapeutic target in both *BRD4*-translocated and *BRD4* wild-type cancers[3,7–12]; at least seven bromodomain inhibitors have reached the clinical stage[13]. Genome-wide studies have identified the role of BRD4-induced epigenetic heterogeneity in cancer cell resistance[14] and factors defining BRD4 inhibitor response[15,16]. However, despite its clinical importance and the broad role of BRD4 in chromatin organization, surprisingly little is known about factors that are directly required for BRD4 function. To systematically expand the list of known BRD4 interactors[5] and characterize proteins directly required for BRD4 function, we developed a strategy of two complementary screens for the genetic and physical partners of BRD4. The two approaches converge on a single factor, MTHFD1. Our description of a transcriptional role for this C-1-tetrahydrofolate synthase highlights a direct connection between nuclear folate metabolism and cancer regulation.

Results

A genetic loss-of-function screen for BRD4 pathway genes identifies MTHFD1. We recently generated reporter for epigenetic drug screening (REDS) cell lines that respond to inhibition of BRD4 with the expression of red fluorescent protein (RFP) (Supplementary Fig. 1)[17]. The near-haploid genotype of these cells, originating from the chronic myeloid leukemia cell line KBM-7, makes them ideally suited for gene trap genetic screens[18,19]. Therefore, we tested several REDS clones for their karyotype and confirmed the haploidy of one clone, REDS1. This clone, which harbors a single RFP integration in the first intron of *CDKAL1*, robustly induced RFP expression when treated with the BRD4 inhibitor (*S*)-JQ1 or with short hairpin RNAs (shRNAs) targeting *BRD4* messenger RNA (Supplementary Fig. 1). We then performed a gene-trap-mediated genetic screen on this

[1]CeMM Research Center for Molecular Medicine of the Austrian Academy of Sciences, Vienna, Austria. [2]Research Institute of Molecular Pathology (IMP), Vienna Biocenter (VBC), Vienna, Austria. [3]Christian Doppler Laboratory for Chemical Epigenetics and Antiinfectives, CeMM Research Center for Molecular Medicine of the Austrian Academy of Sciences, Vienna, Austria. [4]Department of Physiology, Center of Physiology and Pharmacology & Comprehensive Cancer Center, Medical University of Vienna, Vienna, Austria. [5]Department of Medical Oncology, Dana–Farber Cancer Institute, Harvard Medical School, Boston, MA, USA. [6]Institute of Molecular Biotechnology of the Austrian Academy of Sciences (IMBA), Vienna BioCenter (VBC), Vienna, Austria. [7]Department of Biotechnology and Biophysics, Biocenter, University of Würzburg, Würzburg, Germany. [8]Institute of Structural Biology, Rudolf Virchow Center for Experimental Biomedicine, University of Würzburg, Würzburg, Germany. [9]Department of Laboratory Medicine, Medical University of Vienna, Vienna, Austria. [10]Ludwig Boltzmann Institute for Cancer Research, Vienna, Austria. [11]Max Planck Institute for Informatics, Saarbrücken, Germany. [12]Medical University of Vienna, Vienna BioCenter (VBC), Vienna, Austria. [13]Present address: Centre for Genomic Regulation (CRG), The Barcelona Institute of Science and Technology, Barcelona, Spain. [14]Present address: Biochemistry Department, University Stuttgart, Stuttgart, Germany. [15]Present address: Regensburg Center for Interventional Immunology (RCI), University Regensburg and University Medical Center, Regensburg, Germany. *e-mail: skubicek@cemm.oeaw.ac.at

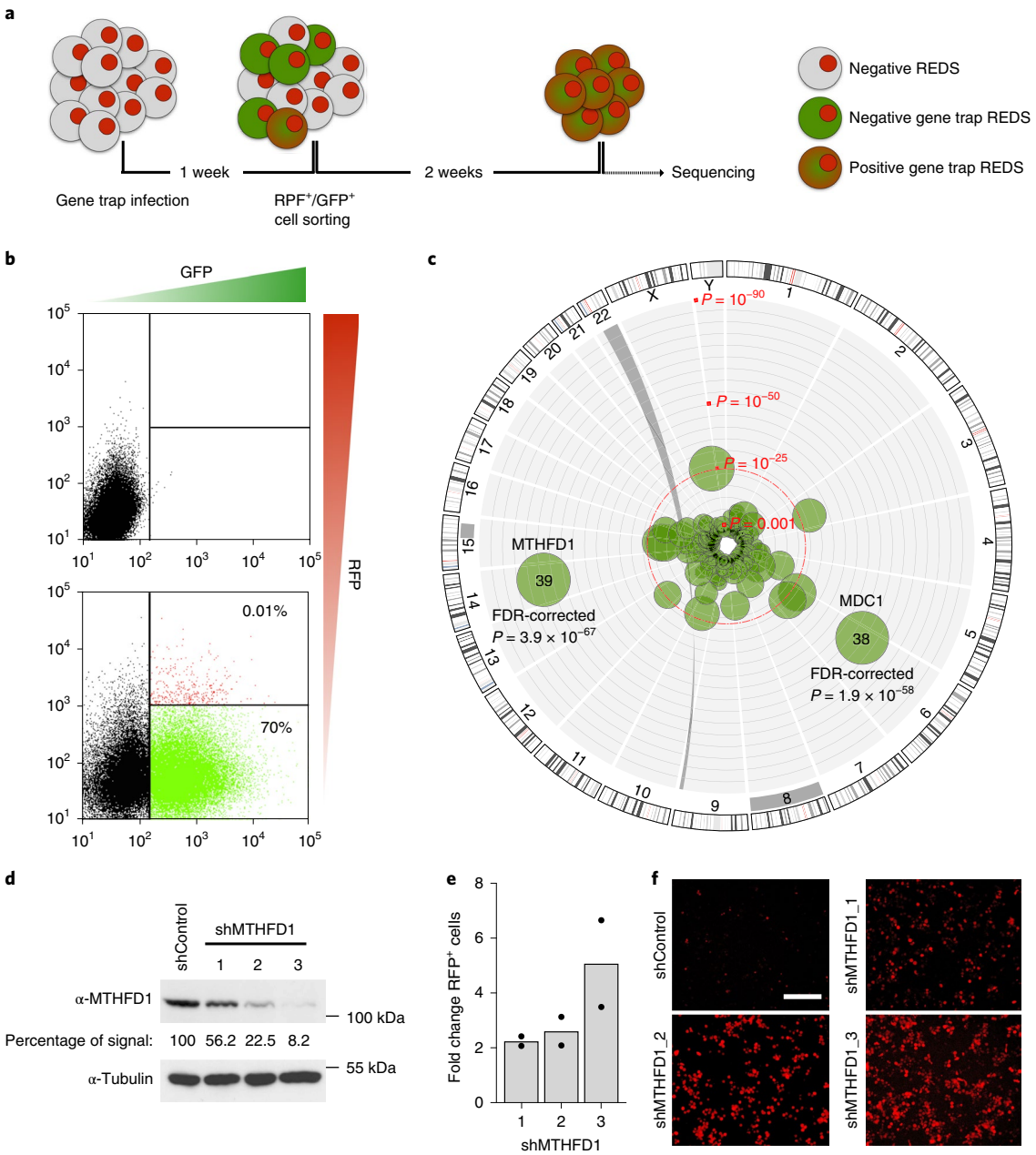

Fig. 1 | A genetic screen identifies MTHFD1 as a functional partner of BRD4. a, Schematic overview of the gene-trap-based genetic screen. **b**, Representative panels of the applied FACS strategy showing non-infected (upper panel) and gene-trap-infected (lower panel) REDS1 cells; infected double-positive (GFP⁺/RFP⁺) cells (shown in red, 0.01%) were sorted. **c**, Circos plot illustrating the results from the gene trap screen by genomic location (outside ring), number of independent inactivating integrations (bubble size) and significance (distance from the center). *P* values were calculated by one-sided Fisher's exact test of insertions over an unselected control dataset adjusted for FDR using the Benjamini–Hochberg procedure. The screen was performed in three biologically independent experiments. **d**, Western blot showing MTHFD1 protein levels after downregulation with the indicated shRNAs in REDS1 cells. The numbers indicate the percentage of MTHFD1 protein remaining; tubulin was used as a loading control. The experiment was repeated three times with similar results. **e**, Quantification of RFP⁺ cells from live cell imaging of REDS1 cells treated with MTHFD1 shRNA. Two biological replicates were analyzed for each experimental condition. **f**, Representative live cell images of MTHFD1 knockdown in REDS1 cells. Scale bar, 100 µm.

clone to identify new functional interactors of BRD4 (Fig. 1a). The high specificity of the screening system relies on a rapid gain of RFP signal, which indicates chromatin changes mimicking BRD4 inhibition. Therefore, the expression of RFP following a specific gene knockout suggests that the gene targeted is either directly required for BRD4 function or independently involved in chromatin remodeling at BRD4-dependent loci. We infected REDS1 cells with a gene trap virus that results in the integration of a splice acceptor site followed by a green fluorescent protein (GFP) reporter gene and a polyadenylation signal, thereby causing the premature termination, typically after the first exon, and thus loss of function of target genes. We then expanded cells for 2 weeks, sorted double-positive cells (RFP⁺/GFP⁺) (Fig. 1b), extracted genomic DNA from this population, amplified gene-trap-integration sites and sequenced and mapped them onto the genome. Two prominent protein-coding genes emerged from the analysis of these data for the number and orientation of integrations: *MTHFD1* and *MDC1* (Fig. 1c, Supplementary Fig. 2 and Supplementary Table 1). *MDC1*, a gene

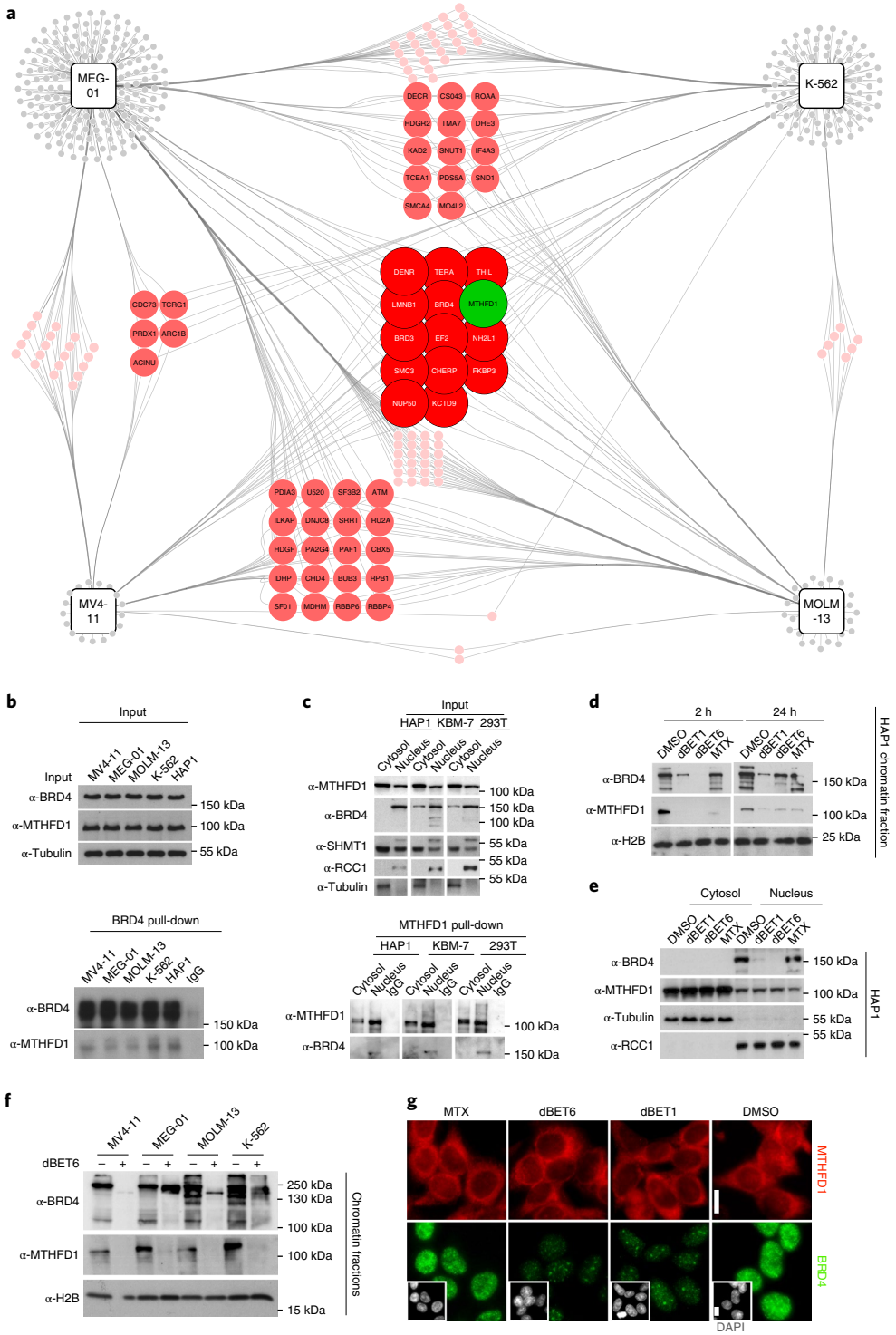

Fig. 2 | BRD4 recruits MTHFD1 to chromatin. a, BRD4 interactomes in MEG-01, K-562, MV4-11 and MOLM-13 cell lines. Proteins are represented as circles; the colors indicate the number of cell lines where a particular interacting protein was detected. **b**, Western blot confirmation of the BRD4-MTHFD1 interaction in leukemia cell lines. The experiment was repeated twice with similar results. **c**, Upper panel: western blot following nuclear versus cytoplasmic fractionation in HAP1, KBM-7 and HEK293T cell lines. RCC1 was used as nuclear loading control while tubulin was used as cytosolic loading control. Lower panel: western blot following MTHFD1 pull-down in the different cell fractions. The experiment was repeated three times with similar results. **d**, Western blot performed on chromatin-associated protein samples extracted from HAP1 cells treated with the indicated compounds for 2 h (dBET1, 0.5 μM; dBET6, 0.5 μM; MTX, 1 μM) or 24 h (dBET1, 0.5 μM; dBET6, 0.05 μM; MTX, 1 μM). H2B antibody was used as the loading control. The experiment was repeated three times with similar results. **e**, Western blot for nuclear versus cytoplasmic protein levels in HAP1 cells treated for 24 h as above. The experiment was repeated twice with similar results. **f**, Western blot from chromatin fractions of MEG-01, K-562, MV4-11 and MOLM-13 cells treated with dBET6 for 2 h. The experiment was repeated twice with similar results. **g**, Immunofluorescence images of HeLa cells treated with the indicated compounds and stained for MTHFD1, BRD4 and DAPI (small inserts). Scale bar, 10 μm.

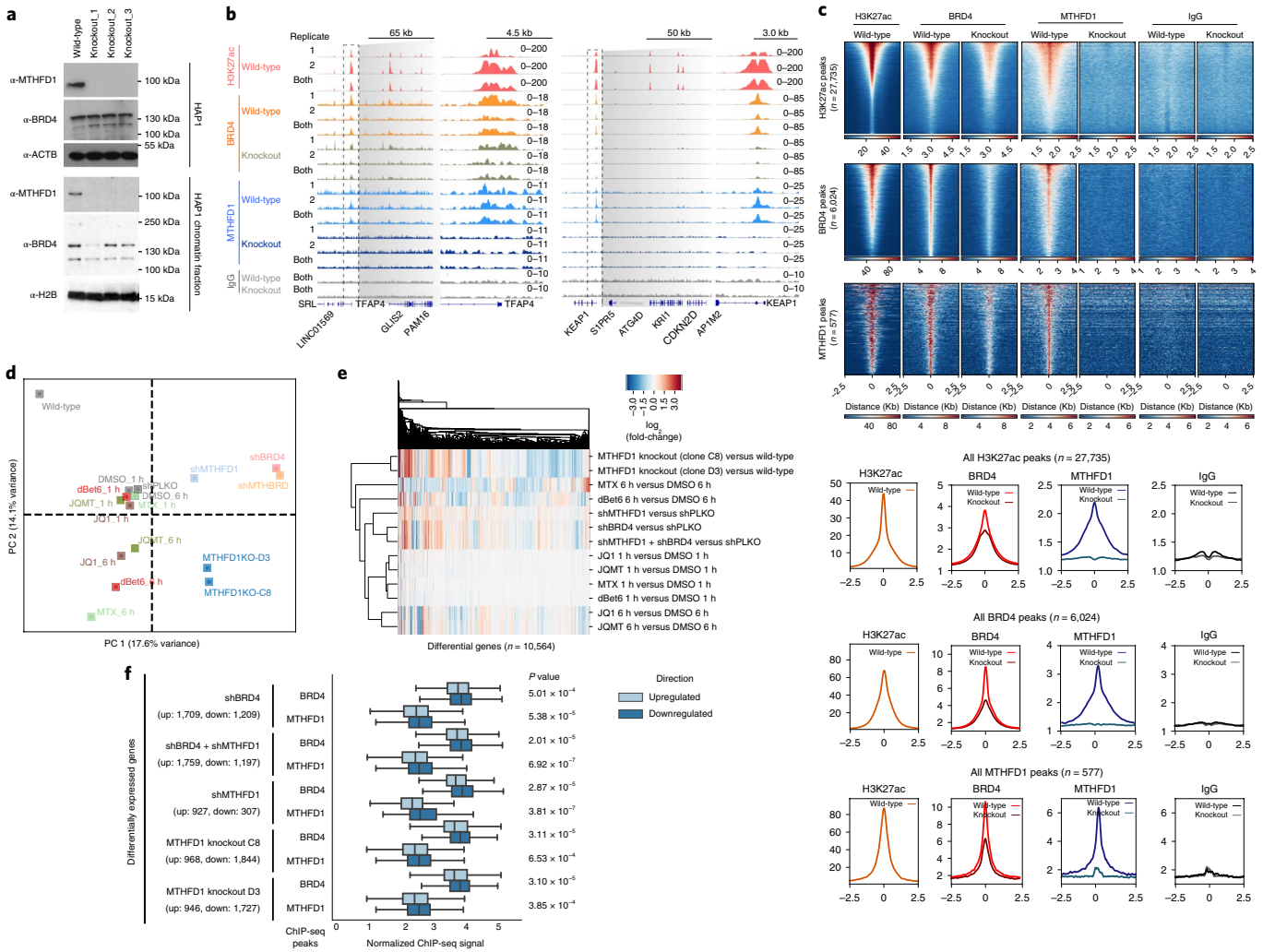

Fig. 3 | MTHFD1 regulates transcription by binding BRD4-occupied chromatin. a, Validation of MTHFD1 knockout HAP1 cell lines. The experiment was repeated three times with similar results. **b**, Representative genome browser view of BRD4, MTHFD1 and H3K27ac binding in the promoters of TFAP4 (left) and KEAP1 (right). All ChIP tracks were normalized to 1× genome coverage. All the immunoprecipitations were performed in biological duplicate. Specifically for MTHFD1 knockout cells, MTHFD1 knockout_1 and MTHFD1 knockout_3 were used as independent biological replicates. **c**, Enrichment of BRD4 and MTHFD1 ChIP signal. Peaks were sorted by total abundance and the data represent merged replicates normalized to 1× genome coverage. **d**, Principal component analysis of RNA-seq data of two MTHFD1 knockout clones and of wild-type HAP1 cells treated with 0.1 μM dBET6, 1 μM (*S*)-JQ1 and 1 μM MTX, shRNAs targeting BRD4 or MTHFD1. Equal amount of dimethylsulfoxide (DMSO) or non-targeting hairpins were used as the respective control conditions; two biological replicates were analyzed for each experimental condition. **e**, Heatmap of relative transcription changes in HAP1 cells compared to the respective control cells. **f**, Integration of ChIP-seq and RNA-seq data in HAP1 cells. BRD4 and MTHFD1 binding at sites associated with genes that are significantly up- or downregulated on knockdown of BRD4 and/or MTHFD1 and in MTHFD1 knockout cells compared to HAP1 wild-type cells. The values represent the estimated factor abundance normalized by matched IgG signal; equality of distributions was assessed with a one-sided Mann–Whitney *U*-test. The boxplot boxes represent the interquartile range with center on median and the whiskers represent values 1.5× outside the respective interquartile ranges.

involved in DNA repair, can be linked to BRD4 biology indirectly through the insulator role of the short isoform of BRD4 during DNA damage signaling[2]. To validate *MTHFD1* as a genetic interactor of BRD4, REDS1 cells were treated with three different shRNAs resulting in 44–92% knockdown of MTHFD1 (Fig. 1d). All three hairpins induced RFP expression; the effect size correlated with their knockdown efficiency (Fig. 1e,f). To rule out clone-specific effects, we repeated the same experiment in the diploid REDS3 clone and obtained comparable results (Supplementary Fig. 2).

MTHFD1 is recruited to chromatin by physical interaction with BRD4. In a second complementary profiling approach, we used proteomics to identify BRD4 interactors in K-562, MOLM-13, MV4-11 and MEG-01 leukemia cell lines (Fig. 2a and Supplementary Fig. 3). Only 13 proteins commonly interacted with BRD4 in all four cell lines. This set comprised several chromatin proteins like BRD3, lamin-B1 and structural maintenance of chromosomes protein 3 and additionally included MTHFD1, the folate pathway enzyme identified in the genetic screen. The physical interaction between BRD4 and MTHFD1 was confirmed in the four leukemia cell lines (Fig. 2b) and all additional cell lines tested (Supplementary Fig. 3). The inverse experiment using MTHFD1 as bait confirmed the interaction with BRD4 and other proteins important for transcription (Supplementary Fig. 3). On tiling peptide microarrays, MTHFD1 interacted with several BRD4-derived peptides, particularly those of the bromodomains (Supplementary Fig. 3). Similarly, several potential interaction sites were identified on MTHFD1, and acetylation of MTHFD1-derived peptides on the known modification

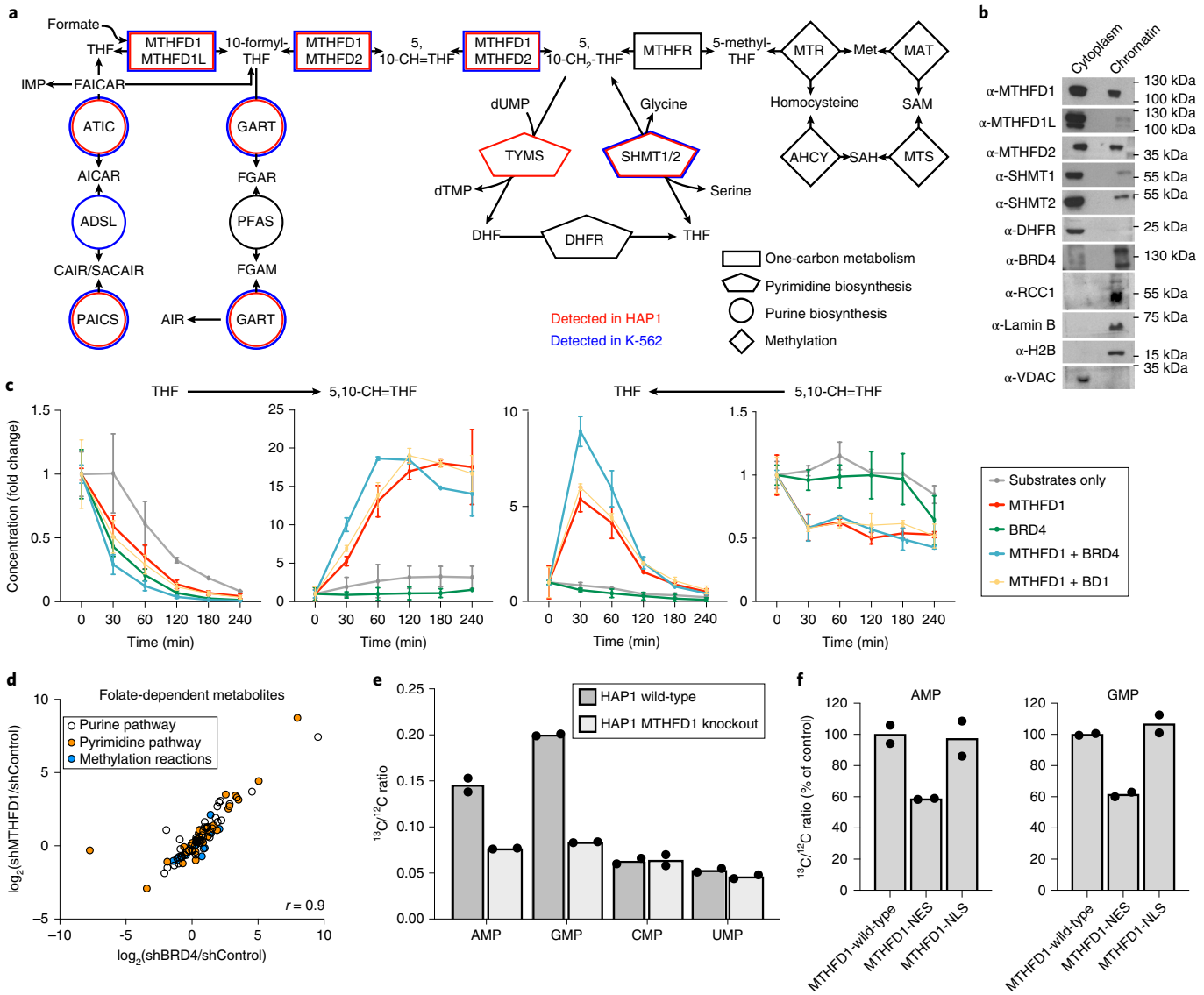

Fig. 4 | Effects of MTHFD1 loss on nuclear metabolite composition. a, Representation of the folate pathway. Enzyme names are reported inside the geometric shapes, connecting the different metabolites. Enzymes associated with chromatin in HAP1 and K-562 cells by MS analysis are indicated in red and blue, respectively. Two biological replicates were analyzed. AICAR, 5-aminoimidazole-4-carboxamide ribonucleotide; AIR, 5-aminoimidizole ribonucleotide; CAIR, 5-aminoimidazole-4-carboxyribonucleotide; dTMP, deoxythymidine monophosphate; dUMP, deoxyuridine monophosphate; FAICAR, 5-formamidoimidazole-4-carboxamide ribotide; FGAM, phosphoribosylformylglycinamidine; FGAR, phosphoribosyl-*N*-formylglycineamide; IMP, inosine monophosphate; MTHFR, methylene tetrahydrofolate reductase; SAH, *S*-adenosyl-L-homocysteine; SAICAR, phosphoribosylaminoimidazolesuccinocarboxamide; SAM, *S*-adenosyl methionine. **b**, Western blot for folate pathway enzymes in the cytoplasmic and chromatin fractions of HAP1 cells. The experiment was repeated twice with similar results. **c**, Recombinant enzyme assays for MTHFD1 activity to convert THF and formate to 5,10-methenyl-THF and vice versa in the presence or absence of full-length BRD4 or its first bromodomain. Mean ± s.d. from $n = 2$ independent samples. **d**, Scatter plot representing metabolite changes in the pyrimidine, purine and methionine biosynthetic pathways on downregulation of BRD4 or MTHFD1 by shRNA. Two biological replicates were analyzed for each experimental condition; *r* indicates the Pearson correlation coefficient. **e**, Incorporation of labeled formate into RNA. HAP1 wild-type and MTHFD1 knockout cells were treated with ^{13}C-labeled sodium formate for 24 h, followed by RNA extraction and LC–MS/MS analysis of nucleotides for the $^{13}C/^{12}C$ ratio. Two biological replicates were analyzed for each experimental condition. AMP, adenosine monophosphate; CMP, cytidine monophosphate; GMP, guanosine monophosphate; UMP, uridine monophosphate. **f**, Incorporation of labeled formate into RNA using the same procedure with MTHFD1 knockout cells transiently transfected with full-length MTHFD1, or the protein with either an NLS or an NES. The percentage of control is calculated considering the ^{13}C incorporation in HAP1 wild-type and MTHFD1 knockout, respectively, as 100% and 0. Two biological replicates were analyzed for each experimental condition.

sites K56 and K819 increased the binding of BRD4. Recombinant MTHFD1 and a MTHFD1 (K56ac) peptide inhibited the interaction between BRD4 and acetylated histone peptides (Supplementary Fig. 3). In cellular pull-down assays, all BRD4 isoforms interacted with full-length MTHFD1 but not with the dehydrogenase/cyclohydrolase or formyltetrahydrofolate synthetase domains alone (Supplementary Fig. 4). The MTHFD1 (K56A) mutation, which mimics the uncharged acetylated state, enhanced interaction with BRD4, while mutation of the same residue to a charged arginine reduced the interaction. An N-terminal BRD4 (1–480) fragment harboring both bromodomains was sufficient for the interaction with full-length MTHFD1, and the double bromodomain mutant

GFP-BRD4 N140F/N433F showed drastically reduced binding to FLAG-MTHFD1 (Supplementary Fig. 4). In summary, these biochemical data are consistent with the interaction between the proteins occurring on several specific contact points, which are enhanced by binding of the BRD4 bromodomains to acetylated lysines on the surface of MTHFD1. Future studies are needed to structurally resolve the configuration of chromatin-bound MTHFD1 and elucidate the impact of BRD4-dependent condensates[20,21] on the interaction.

While BRD4 is localized almost exclusively to the nucleus, folate metabolism is considered to occur in the cytoplasm and mitochondria[22]. Nuclear import of folate pathway enzymes including MTHFD1 has been described only recently[23,24]. Nuclear versus cytosolic fractionation of HAP1, KBM-7 and HEK293T cells indicated that a fraction of MTHFD1 resides in the nucleus in all three cell lines (Fig. 2c). MTHFD1 pull-downs in the cytosolic and nuclear fractions of HAP1, KBM-7 and HEK293T revealed that the interaction with BRD4 was restricted to the nucleus (Fig. 2c). With the nucleus confirmed as the interaction site of BRD4 and MTHFD1, we asked whether the BRD4-MTHFD1 complex was chromatin-bound or rather found in the soluble nuclear faction. We prepared chromatin extracts comprising tightly DNA-bound proteins from HAP1 cells and checked for the presence of BRD4 and MTHFD1 by western blotting. Both proteins were clearly detectable in the chromatin-bound fraction (Fig. 2d). To probe whether BRD4 recruits MTHFD1 to chromatin, we treated HAP1 cells with the small molecule degronimids dBET1 (ref. [25]) and dBET6 (ref. [4]). Two-hour treatment with these compounds resulted in the nearly complete ablation of BRD4 from chromatin. Under these conditions, MTHFD1 was lost from chromatin, with remaining levels correlating with the amount of BRD4 (Fig. 2d), suggesting that BRD4 is the main factor recruiting MTHFD1 to chromatin. We further observed that methotrexate (MTX), an antifolate acting primarily on dihydrofolate reductase (DHFR), caused a similar depletion of chromatin-associated MTHFD1, while it did not affect BRD4 levels. A possible explanation is direct competition between BRD4 and MTX for binding to the MTHFD1 substrate pocket containing K56ac. Importantly, BRD4 degradation or MTX treatment did not impair MTHFD1 nuclear localization (Fig. 2e), suggesting that while nuclear import of MTHFD1 is otherwise mediated, the interaction with BRD4 accounts for the recruitment of MTHFD1 to chromatin. To ensure cell-type independence, we confirmed that BRD4 degradation results in loss of MTHFD1 from chromatin in five additional cell lines (Fig. 2f,g).

Colocalization of MTHFD1 and BRD4 regulates gene expression. Having characterized BRD4-dependent chromatin recruitment of MTHFD1, we aimed to identify the genomic location of MTHFD1 binding by mapping the binding sites of the enzyme by chromatin immunoprecipitation sequencing (ChIP-seq) experiments in HAP1 cells. To control for antibody specificity, we generated MTHFD1-null HAP1 cells by CRISPR–Cas9 genome editing (Fig. 3a and Supplementary Fig. 5). MTHFD1 was detected at distinct genomic loci and signal was lost in MTHFD1 knockout cells (Fig. 3b). In line with the proteomics experiments, the vast majority of MTHFD1 binding sites overlapped with BRD4 binding sites at promoter and enhancer regions, where H3K27ac was also enriched (Fig. 3c and Supplementary Fig. 6). Importantly, MTHFD1 chromatin binding was also lost after acute BRD4 degradation by 2 h treatment with dBET6 (Supplementary Fig. 7), suggesting a widespread role of MTHFD1 in chromatin regulation. Transcriptome analysis of HAP1 cells treated with BRD4 inhibitors, degraders and antifolates, as well as genetic perturbation by knockdown of BRD4 and knockdown/knockout of MTHFD1 validated the respective perturbation (Supplementary Fig. 8). While MTHFD1 knockout resulted in expression changes of additional genes in the folate pathway, the more acute perturbations by compounds and shRNAs caused only minor changes in these genes. On the whole transcriptome level, we observed agreement in gene expression changes of compounds targeting BRD4 and antifolates, as well as between the genetic perturbation of BRD4 and MTHFD1 (Fig. 3d,e). Both MTHFD1 and BRD4 binding sites were enriched in promoters of genes with transcriptional functions (Supplementary Fig. 6); combined analysis of chromatin binding and transcriptome changes revealed that genes bound by either protein were more highly expressed compared to similar genes without binding as detected by ChIP-seq (Supplementary Fig. 8). Both MTHFD1 and BRD4 were enriched at promoters of genes that were downregulated following knockdown of either of these proteins (Fig. 3f and Supplementary Fig. 8). The correlation between transcriptional effects of bromodomain and extra-terminal (BET) inhibitors and antifolates, as well as between knockdown of MTHFD1 and BRD4 was conserved in K-562 and A549 cells, suggesting cell-type independence (Supplementary Fig. 9).

Loss of MTHFD1 or BRD4 results in similar metabolic changes. MTHFD1 is a C-1-tetrahydrofolate synthase that catalyzes three enzymatic reactions in folate metabolism, resulting in the interconversion of tetrahydrofolate (THF), 10-formyl-THF, 5,10-methenyltetrahydrofolate (5,10-CH=THF) and 5,10-methylenetetrahydrofolate (5,10-CH_2-THF) (Fig. 4a). These folates are key intermediates of one-carbon metabolism and provide activated C1 groups for the biosynthesis of purines, pyrimidines and methionines. Biosynthesis of these three major classes of C1 metabolism products is considered to occur predominantly in the cytoplasm and mitochondria of mammalian cells[22], but we detected not only MTHFD1 but also several other enzymes required for nucleotide biosynthesis in the tightly chromatin-associated protein fraction in K-562 and HAP1 cells (Fig. 4a,b and Supplementary Table 2). To test whether BRD4 might affect MTHFD1 enzymatic activity, we used enzyme assays with recombinant protein in the presence of either full-length BRD4 or only the first bromodomain. We observed that full-length BRD4 boosted the activity of MTHFD1 to convert THF to 5,10-CH=THF (Fig. 4c).

We next asked whether inhibition of BRD4 or MTHFD1 altered nuclear metabolite composition. To reduce technical challenges by fast diffusion rates and unselective metabolite loss through the nuclear pore as much as possible, we used a protocol of rapid nuclei isolation after knockdown of either BRD4 or MTHFD1, and analyzed the nuclear metabolome relative to a non-targeting control hairpin. In total, we detected 2,851 metabolites, of which over 400 were significantly changed in one of the conditions. We observed strong correlation between the nuclear metabolomes in BRD4 and MTHFD1 knockdown conditions, particularly for metabolites in the purine, pyrimidine and methionine biosynthesis pathways (Fig. 4d and Supplementary Fig. 10). The direct MTHFD1 product 5,10-CH_2-THF and most of the precursors for de novo nucleoside and nucleotide biosynthesis were depleted in both conditions, whereas the vast majority of free bases, nucleosides and nucleotides were increased. Furthermore, the trend for similar changes in nuclear metabolite composition was also noticeable in cells treated with the small molecules dBET1 and MTX (Supplementary Fig. 10). BET inhibitors and MTX caused highly correlated characteristic changes specifically in the nuclear folate pool that were not observed with other cytotoxic compounds (Supplementary Fig. 10). Overall, a common nuclear metabolite signature for the inhibition of MTHFD1 and of BRD4 is evident, indicating a crosstalk between BRD4-dependent epigenetic regulation and folate metabolism. To test whether MTHFD1-derived metabolites are converted into nucleotides and incorporated into RNA, we treated cells with stable isotope-labeled sodium formate-^{13}C, a co-substrate for the conversion of THF to 10-formyl-THF. Within 2 h we observed label incorporation into the direct MTHFD1

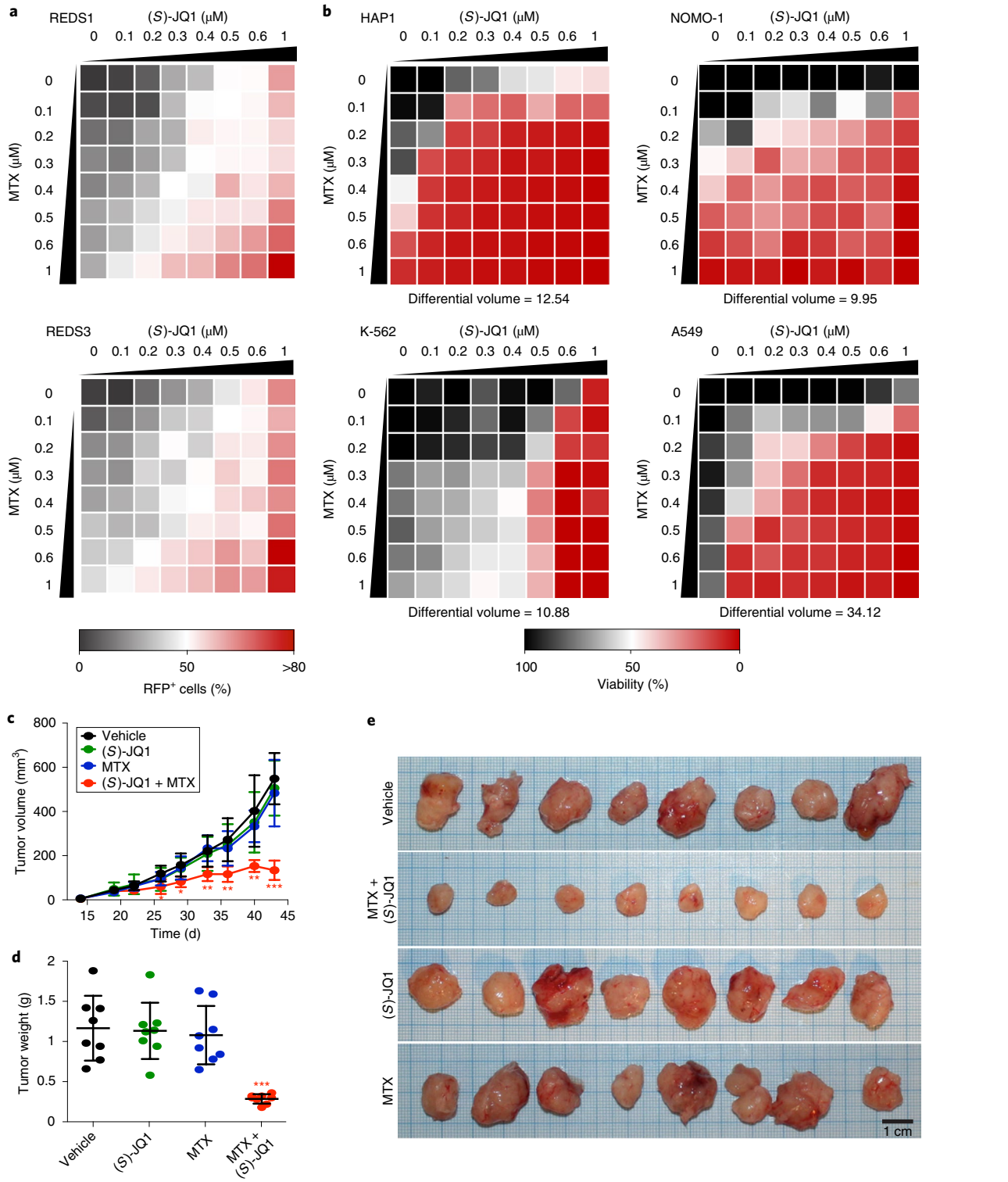

Fig. 5 | BET bromodomain inhibitors synergize with antifolates to impair cancer cell growth. a, Dose–response matrix displaying REDS1 and REDS3 RFP$^+$ cells treated with the indicated concentrations of (*S*)-JQ1 and MTX alone or in combination. The means from two biological replicates are shown. **b**, Dose–response matrices displaying the cell viability of HAP1, NOMO-1, K-562 and A549 treated for 72 h with (*S*)-JQ1 and MTX alone or in combination. The means from two biological replicates are shown. The differential volume indicates the sum of all deviations from Bliss additivity over the dose–response matrix. **c**, Tumor volumes from an A549 xenograft mouse model treated 5 times per week with 30 mg kg^{-1} (*S*)-JQ1 and/or twice weekly with 25 mg kg^{-1} MTX from day 19. The means and standard deviations from eight mice per group are shown. The asterisks indicate the significance of a one-way analysis of variance (ANOVA) adjusted by Tukey's multiple comparison test (*$P < 0.05$; **$P < 0.005$; ***$P < 0.0001$) **d**, Weight of tumors at the end of the experiment (day 43). The means and standard deviations from eight mice per group are shown. The asterisks indicate the significance of a one-way ANOVA adjusted by Tukey's multiple comparison test ($P = 0.00000050$). **e**, Images of tumors at the end of the experiment (day 43).

products 5,10-CH=THF and 5,10-CH_2-THF in wild-type HAP1 cells (Supplementary Fig. 10f). In MTHFD1 knockout HAP1 cells, both the levels and the relative label incorporation of these metabolites were strongly reduced. We then isolated and hydrolyzed total cellular RNA after 24 h of sodium formate-^{13}C treatment. In wild-type HAP1 cells we observed significant label incorporation in purine but not pyrimidine nucleotides, which was absent in MTHFD1 knockout cells (Fig. 4e). Therefore, we reconstituted MTHFD1 knockout cells with either wild-type MTHFD1 or versions of the enzyme with constitutive nuclear localization (NLS) and nuclear export (NES) signals (Supplementary Fig. 11). Wild-type and NLS MTHFD1 resulted in label incorporation to levels comparable to HAP1 wild-type cells. In contrast, cytoplasm-enriched MTHFD1-NES resulted in lower levels of formate-derived purine bases incorporated into RNA, arguing for a nuclear-specific role of MTHFD1 (Fig. 4f).

Antifolates synergize with BRD4 inhibitors in diverse cancer models. Based on the similarities in nuclear metabolite composition following loss of MTHFD1 and BRD4, we speculated that antifolates might synergize with BRD4 inhibitors. To test this hypothesis, we treated REDS cells with (*S*)-JQ1 and MTX alone and in combination. Co-treatment with MTX remarkably amplified the basal RFP signal given by low doses of (*S*)-JQ1 alone (Fig. 5a). These results indicate that the chromatin remodeling process can be enhanced when inhibiting BRD4 and MTHFD1 together, emphasizing the role of folate metabolites in epigenetic regulation. We next tested whether this drug synergy also affected cancer cell survival. We selected six cell lines including four cell lines described as not sensitive to BRD4 inhibition, plus KBM-7 and HAP1 cells (Supplementary Fig. 12). Dose–response curves confirmed the low sensitivity of these cell lines to (*S*)-JQ1 treatment and a moderate-to-low sensitivity to MTX treatment (Supplementary Fig. 12). In contrast to the poor response to (*S*)-JQ1 and MTX individual treatments, the combination of both drugs efficiently impaired cell viability in all six cell lines tested (Fig. 5b and Supplementary Fig. 12). Toxicity was observed at concentrations without any single-agent activity, indicating strong synergy between the two treatments, which was confirmed by calculating synergy indices according to the Bliss independence model[26] (Supplementary Fig. 12d). To exclude possible off-target effects of MTX, we treated the cell line showing the strongest drug synergism, A549, with shRNA for MTHFD1 and demonstrated increased sensitivity to (*S*)-JQ1 (Supplementary Fig. 12e). In addition, MTHFD1 knockout HAP1-null cells responded with the induction of apoptosis at lower concentrations of (*S*)-JQ1 and MTX compared to wild-type cells (Supplementary Fig. 12). We further established that BET bromodomain inhibitors can be combined with antifolates in vivo to specifically inhibit cancer cell proliferation without exerting general toxicity. When we treated an A549 xenograft mouse model[27] with MTX and (*S*)-JQ1 alone and in combination, tumor growth was not impaired by either of the individual compounds, but arrested when the two inhibitors were given together (Fig. 5c–e).

Discussion

In contrast to nuclear ATP and acetyl coenzyme A biosynthesis[28,29], a direct role of folate pathway enzymes in the control of gene expression has not been comprehensively investigated. In this study, we characterize a transcriptional role for nuclear folate metabolism based on the genetic and biochemical interaction of MTHFD1 with BRD4. A fraction of MTHFD1 has previously been shown to reside in the nucleus where it is critical for thymidylate biosynthesis and protection from DNA damage response following folate deficiency[23,30–32]. In the current study, we show that MTHFD1 binds chromatin in a BRD4-dependent manner at distinct genomic loci, where it controls gene expression and maintains a pool of folate metabolites in the nucleus. Interestingly, we identified not only MTHFD1 but also the other enzymes of the de novo nucleotide biosynthesis pathway physically bound to chromatin. These enzymes were also detected in a recent large-scale chromatin proteomics study[33] and the purine pathway enzymes SHMT and ADE2 have been described as direct interactors of the BRD4 bromodomains[34]. Purine nucleotides are also the metabolites we find most dramatically changed following loss of either BRD4 or MTHFD1. While purine biosynthesis is generally considered to be localized exclusively to the cytoplasm, early work has shown that radioactive formate can be incorporated into RNA purine bases by isolated nuclei[35]. Future experiments will need to carefully evaluate the enzymatic activity of chromatin-bound nucleotide biosynthetic enzymes to uncover if certain steps of the pathway can also occur within the nucleus. In addition to the direct requirement of nucleotides for transcription, alterations in thymidylate and purine biosynthesis downstream of MTFHD1 might also cause nucleotide stress, which is known to impair P-TEFb activation and transcriptional elongation via upregulation of protein HEXIM1 (ref. [36]). We hypothesize that BRD4-dependent MTHFD1 recruitment is needed to support local availability of one-carbon metabolites for full transcriptional activation of certain BRD4 target genes needed for cancer cell proliferation. Thus, our finding adds to the growing list of metabolic enzymes and metabolites with roles in the regulation of chromatin structure and transcription[37–40].

Due to its fundamental role in cell proliferation via nucleic acid biosynthesis, folate metabolism has been widely investigated in cancer biology. Several small molecules, including MTX, that target different enzymes of the folate pathway[41] have been developed. These antifolates are considered to act by inhibiting cell division, DNA/RNA synthesis and repair and protein synthesis[42]. Our findings suggest an additional 'targeted' mode of these classical chemotherapeutic drugs, which could enable better stratification and treatment regimens for cancer patients. Furthermore, we suggest combination of antifolates with BRD4 inhibitors as possible treatment for particularly aggressive cancers, potentially opening the avenue for more successful therapies.

Online content

Any methods, additional references, Nature Research reporting summaries, source data, statements of code and data availability and associated accession codes are available at https://doi.org/10.1038/s41588-019-0413-z.

Received: 18 April 2018; Accepted: 4 April 2019;
Published online: 27 May 2019

References

1. Filippakopoulos, P. et al. Histone recognition and large-scale structural analysis of the human bromodomain family. *Cell* **149**, 214–231 (2012).
2. Floyd, S. R. et al. The bromodomain protein Brd4 insulates chromatin from DNA damage signalling. *Nature* **498**, 246–250 (2013).
3. Filippakopoulos, P. et al. Selective inhibition of BET bromodomains. *Nature* **468**, 1067–1073 (2010).
4. Winter, G. E. et al. BET bromodomain proteins function as master transcription elongation factors independent of CDK9 recruitment. *Mol. Cell* **67**, 5–18.e19 (2017).
5. Shi, J. & Vakoc, C. R. The mechanisms behind the therapeutic activity of BET bromodomain inhibition. *Mol. Cell* **54**, 728–736 (2014).
6. Zhou, Q., Li, T. & Price, D. H. RNA polymerase II elongation control. *Annu. Rev. Biochem.* **81**, 119–143 (2012).
7. Asangani, I. A. et al. Therapeutic targeting of BET bromodomain proteins in castration-resistant prostate cancer. *Nature* **510**, 278–282 (2014).
8. Dawson, M. A. et al. Inhibition of BET recruitment to chromatin as an effective treatment for MLL-fusion leukaemia. *Nature* **478**, 529–533 (2011).
9. Delmore, J. E. et al. BET bromodomain inhibition as a therapeutic strategy to target c-Myc. *Cell* **146**, 904–917 (2011).
10. Lovén, J. et al. Selective inhibition of tumor oncogenes by disruption of super-enhancers. *Cell* **153**, 320–334 (2013).
11. Shu, S. et al. Response and resistance to BET bromodomain inhibitors in triple-negative breast cancer. *Nature* **529**, 413–417 (2016).
12. Zuber, J. et al. RNAi screen identifies Brd4 as a therapeutic target in acute myeloid leukaemia. *Nature* **478**, 524–528 (2011).

13. Filippakopoulos, P. & Knapp, S. Targeting bromodomains: epigenetic readers of lysine acetylation. *Nat. Rev. Drug Discov.* **13**, 337–356 (2014).
14. Knoechel, B. et al. An epigenetic mechanism of resistance to targeted therapy in T cell acute lymphoblastic leukemia. *Nat. Genet.* **46**, 364–370 (2014).
15. Rathert, P. et al. Transcriptional plasticity promotes primary and acquired resistance to BET inhibition. *Nature* **525**, 543–547 (2015).
16. Fong, C. Y. et al. BET inhibitor resistance emerges from leukaemia stem cells. *Nature* **525**, 538–542 (2015).
17. Sdelci, S. et al. Mapping the chemical chromatin reactivation landscape identifies BRD4-TAF1 cross-talk. *Nat. Chem. Biol.* **12**, 504–510 (2016).
18. Carette, J. E. et al. Haploid genetic screens in human cells identify host factors used by pathogens. *Science* **326**, 1231–1235 (2009).
19. Tchasovnikarova, I. A. et al. Epigenetic silencing by the HUSH complex mediates position-effect variegation in human cells. *Science* **348**, 1481–1485 (2015).
20. Sabari, B. R. Coactivator condensation at super-enhancers links phase separation and gene control. *Science* **361**, eaar3958 (2018).
21. Cho, W. K. et al. Mediator and RNA polymerase II clusters associate in transcription-dependent condensates. *Science* **361**, 412–415 (2018).
22. Ducker, G. S. & Rabinowitz, J. D. One-carbon metabolism in health and disease. *Cell Metab.* **25**, 27–42 (2017).
23. Field, M. S. et al. Nuclear enrichment of folate cofactors and methylenetetrahydrofolate dehydrogenase 1 (MTHFD1) protect de novo thymidylate biosynthesis during folate deficiency. *J. Biol. Chem.* **289**, 29642–29650 (2014).
24. Field, M. S., Kamynina, E. & Stover, P. J. MTHFD1 regulates nuclear de novo thymidylate biosynthesis and genome stability. *Biochimie* **126**, 27–30 (2016).
25. Winter, G. E. et al. Phthalimide conjugation as a strategy for in vivo target protein degradation. *Science* **348**, 1376–1381 (2015).
26. Bliss, C. I. The toxicity of poisons applied jointly. *Ann. Appl. Biol.* **26**, 585–615 (1939).
27. Grabner, B. et al. Disruption of STAT3 signalling promotes KRAS-induced lung tumorigenesis. *Nat. Commun.* **6**, 6285 (2015).
28. Wright, R. H. et al. ADP-ribose-derived nuclear ATP synthesis by NUDIX5 is required for chromatin remodeling. *Science* **352**, 1221–1225 (2016).
29. Mews, P. et al. Acetyl-CoA synthetase regulates histone acetylation and hippocampal memory. *Nature* **546**, 381–386 (2017).
30. Kamynina, E. et al. Arsenic trioxide targets MTHFD1 and SUMO-dependent nuclear de novo thymidylate biosynthesis. *Proc. Natl Acad. Sci. USA* **114**, E2319–E2326 (2017).
31. MacFarlane, A. J. et al. Nuclear localization of de novo thymidylate biosynthesis pathway is required to prevent uracil accumulation in DNA. *J. Biol. Chem.* **286**, 44015–44022 (2011).
32. Field, M. S., Kamynina, E., Chon, J. & Stover, P. J. Nuclear folate metabolism. *Annu. Rev. Nutr.* **38**, 219–243 (2018).
33. Ginno, P. A., Burger, L., Seebacher, J., Iesmantavicius, V. & Schübeler, D. Cell cycle-resolved chromatin proteomics reveals the extent of mitotic preservation of the genomic regulatory landscape. *Nat. Commun.* **9**, 4048 (2018).
34. Sudhamalla, B., Dey, D., Breski, M., Nguyen, T. & Islam, K. Site-specific azide-acetyllysine photochemistry on epigenetic readers for interactome profiling. *Chem. Sci.* **8**, 4250–4256 (2017).
35. Perretta, M. & Romero, A. De novo RNA biosynthesis in isolated bone marrow nuclei. *Experientia* **29**, 39–40 (1973).
36. Tan, J. L. et al. Stress from nucleotide depletion activates the transcriptional regulator HEXIM1 to suppress melanoma. *Mol. Cell* **62**, 34–46 (2016).
37. Sharma, U. & Rando, O. J. Metabolic inputs into the epigenome. *Cell Metab.* **25**, 544–558 (2017).
38. Li, X., Egervari, G., Wang, Y., Berger, S. L. & Lu, Z. Regulation of chromatin and gene expression by metabolic enzymes and metabolites. *Nat. Rev. Mol. Cell Biol.* **19**, 563–578 (2018).
39. Boukouris, A. E., Zervopoulos, S. D. & Michelakis, E. D. Metabolic enzymes moonlighting in the nucleus: metabolic regulation of gene transcription. *Trends Biochem. Sci.* **41**, 712–730 (2016).
40. van der Knaap, J. A. & Verrijzer, C. P. Undercover: gene control by metabolites and metabolic enzymes. *Genes Dev.* **30**, 2345–2369 (2016).
41. Anderson, A. C. & Wright, D. L. Antifolate agents: a patent review (2010–2013). *Expert Opin. Ther. Pat.* **24**, 687–697 (2014).
42. Wilson, P. M., Danenberg, P. V., Johnston, P. G., Lenz, H. J. & Ladner, R. D. Standing the test of time: targeting thymidylate biosynthesis in cancer therapy. *Nat. Rev. Clin. Oncol.* **11**, 282–298 (2014).

Acknowledgements

S. Sdelci is a JDRF postdoctoral fellow (no. 3-PDF-2014-206-A-N). D.L.B. is a Merck Fellow of the Damon Runyon Cancer Research Foundation (no. DRG-2196-14). Next-generation sequencing was performed by the Biomedical Sequencing Facility at the CeMM. Research in the Kubicek laboratory is supported by the Austrian Federal Ministry for Digital and Economic Affairs and the National Foundation for Research, Technology, and Development, the Austrian Science Fund (FWF; no. F4701) and the European Research Council (ERC) under the European Union's Horizon 2020 research and innovation program (no. ERC-CoG-772437). Research in the Zuber laboratory was supported by the ERC (no. ERC-StG-336860 to J.Z.), a Research Fellowship of the EU (Marie Curie Actions 329492 to P.R.) and generous institutional funding from Boehringer Ingelheim. We thank all the members of the BioOptic Facility of the Research Institute of Molecular Pathology and the Institute of Molecular Biotechnology GmbH for their help with cell sorting, P. Stover (Cornell) and S. Nijman (Oxford) for kindly providing the plasmids, and A. Terenzi (Donostia International Physics Center) for advice on in vitro metabolomics.

Author contributions

S. Sdelci and S.K. conceived the project and designed the study. S. Sdelci and G.H. performed the gene trap screen. F.S. and R.K. analyzed the gene trap screening data. P.R., O.H., R.I., K.M. and J.Z. performed and analyzed the BRD4 interactome screen. S. Sdelci, W.Y., J.-M.G.L., G.H., A. Ringler and S. Schick performed the biochemical and cell biology experiments and generated the ChIP-seq and metabolomics samples. K.K, B.G. and A.M. performed and analyzed the proteomics and metabolomics experiments. A. Rendeiro, M.O., C.S, M.F., M.S., T.P. and C.B. performed the next-generation sequencing and analyzed the ChIP-seq data. F.K. performed the molecular modeling. P.M., M.O., K.P. and K.L.B. generated and analyzed the chromatin-bound proteomes. P.B. and J.M. analyzed the metabolomics data. S.Y.W. and H.M.M. designed, performed and analyzed the peptide microarray studies. D.L.B., J.E.B. and G.E.W. designed, synthesized and provided the degronimids. H.P.M. and E.C. designed and conducted the mouse xenograft studies. S. Sdelci and S.K. wrote the manuscript with input from all coauthors.

Competing interests

S. Sdelci and S.K. have filed patent application WO/2018/087401 based on the findings described in this manuscript. J.E.B. is now a shareholder and executive of Novartis AG, and was formerly the founder of the BET bromodomain-focused company Tensha (acquired by Roche).

Additional information

Supplementary information is available for this paper at https://doi.org/10.1038/s41588-019-0413-z.

Reprints and permissions information is available at www.nature.com/reprints.

Correspondence and requests for materials should be addressed to S.K.

Publisher's note: Springer Nature remains neutral with regard to jurisdictional claims in published maps and institutional affiliations.

Methods

Cell culture and transfection. Human chronic myelogenous leukemia (KBM-7), biphenotypic B myelomonocytic leukemia (MV4-11), chronic myelogenous leukemia (MEG-01 and K-562) and KBM-7-derived (HAP1) cell lines were cultured in IMDM (Gibco) supplemented with 10% FCS (Gibco). Human embryonic kidney (HEK293T) and cervix adenocarcinoma (HeLa) cell lines were cultured in DMEM (Gibco) supplemented with 10% FCS. Human acute monocytic leukemia (MOLM-13), acute monocytic leukemia (NOMO-1) and lung carcinoma (A549) cell lines were cultured in Roswell Park Memorial Institute 1640 medium (Gibco) supplemented with 10% FCS. All the mentioned cell lines were incubated in 5% CO_2 at 37 °C.

HEK293T cells were transfected with Lipofectamine 2000 (Invitrogen) according to the manufacturer's instructions.

The retroviral gene trap vector (pGT-GFP) was a kind gift from S. Nijman. The GFP-MTHFD1 plasmid was a kind gift from P. Stover.

Western blot analysis and immunoprecipitation. For the western blot analysis, proteins were separated on polyacrylamide gels with SDS running buffer (50 mM Tris, 380 mM glycine, 7 mM SDS) and transferred to nitrocellulose blotting membranes. All membranes were blocked with blocking buffer (5% (m/v) milk powder (BioRad)) in Tris-buffered saline with Tween: 50 mM Tris, 150 mM NaCl, 0.05% (v/v) Tween 20, adjusted to pH 7.6. Proteins were probed with antibodies (sourced from Abcam unless otherwise stated) to BRD4 (1:1,000, catalog no. ab128874), β-actin (1:1,000, catalog no. ab16039), MTHFD1 (catalog no. ab70203; H120, Santa Cruz Biotechnology, catalog no. sc-134732; A8, Santa Cruz, catalog no. sc-271412; all used at 1:1,000), MTHFD1L (1:1,000, catalog no. ab229708), MTHFD2 (1:1,000, catalog no. ab151447), GFP (1:1,000, catalog no. G10362; Thermo Fisher Scientific), regulator of chromosome condensation (RCC1 (C-20), 1:1,000, catalog no. sc-1162; Santa Cruz Biotechnology), β-tubulin (1:1,000, catalog no. T4026; Sigma-Aldrich), SHMT1 (1:1,000, catalog no. ab186130), SHMT2 (1:1,000, catalog no. ab180786), DHFR (1:1,000, catalog no. ab49881), lamin B1 (1:1,000, catalog no. ab16048), VDAC1 (1:1,000, catalog no. ab15895) and histone H2B (1:1,000, catalog no. ab156197) and detected by horseradish peroxidase-conjugated donkey anti-rabbit immunoglobulin G (IgG) antibody (1:5,000, catalog no. ab16284) or Pierce donkey anti-mouse IgG antibody (Thermo Fisher Scientific) and visualized with the Pierce ECL Western Blotting Substrate (Thermo Fisher Scientific), according to the protocol provided. Supplementary Fig. 13 contains full scans of all western blots.

For immunoprecipitation, 1 or 0.5 mg of protein extract was incubated overnight at 4 °C with 10 µl Protein A or G beads (Thermo Fisher Scientific) preincubated for 2 h at 4 °C with 1 µg of BRD4, MTHFD1 (A8) or GFP antibodies.

Gene trap genetic screening. The pGT-GFP vector contains an inactivated 3′ long terminal repeat, a strong adenoviral (Ad40) splice acceptor site, the GFP coding sequence and the simian vacuolating virus 40 polyadenylation signal. The gene trap virus was produced by transfection of 293T cells in T150 dishes with pGT-GFP combined with retroviral packaging plasmids. The virus-containing supernatant was collected after 30, 48 and 72 h of transfection and concentrated using ultracentrifugation for 1.5 h at 24,100 r.p.m. in a Beckman Coulter Optima L-100 XP Ultracentrifuge using an SW 32 Ti Rotor (Beckman Coulter Life Sciences).

For each replicate, 20 million REDS1 cells were mutagenized in a 24-well plate, seeding 1 million cells per well and using spin infection for 45 min at 2,000 r.p.m. Gene-trap-infected cells were assessed by FACS to determine the percentage of infection (percentage of GFP$^+$ cells). If such a percentage was >70%, REDS1 GFP$^+$/RFP$^+$ cells were sorted and left in culture for 2 weeks to get the sufficient number of cells to process for DNA library preparation.

Gene trap analysis. Raw sequencing data were aligned to the human reference genome hg19 (University of California, Santa Cruz hg19 build) using bowtie2 v.2.2.4 with default parameters. Reads that did not meet the following criteria were removed: (1) had a reported alignment—'mapped reads'; (2) had a unique alignment; and (3) had a mapping quality higher than 20. Duplicate reads were marked and discarded with Picard Tools v.1.111. Insertions in close proximity (1 or 2 base pair (bp) distance from each other) were removed to avoid inclusion of insertions due to mapping errors. Insertions were annotated with gene build GRCh37.p13 (Ensembl 75, February 2014 release) using bedtools v.2.10.1 and custom scripts. The canonical transcripts (according to Ensembl) for each gene were used as a reference gene model to count insertions falling with exons, introns or intragenic. Insertions were considered mutagenic or disruptive to the gene if they occurred within exons irrespective of their orientation to the corresponding gene or if they were located within introns in sense orientation[43]. Insertions in the antisense direction with regard to gene orientation were considered silent. All mutagenic insertions were summarized independently for each gene. For each gene, a one-sided Fisher's exact test was applied to estimate a significant enrichment of insertions over an unselected control dataset. Resulting *P* values were adjusted for false discovery rate (FDR) using the Benjamini–Hochberg procedure. A cutoff of 5% FDR indicated that a gene was considered significantly enriched. Insertion plots were drawn with the R software and Circos plots were produced using Circos v.0.69-6 (ref. [44]).

DNA library preparation. DNA was extracted from 30 million GFP$^+$/RFP$^+$ REDS1 cells using the genomic DNA isolation QIAamp DNA Mini Kit (QIAGEN); 4 µg of DNA was digested with NlaIII or MseI (New England Biolabs; four digestions for each enzyme). After spin column purification (QIAGEN QIAquick PCR purification column, catalog no. 28115), 1 µg of digested DNA was ligated using T4 DNA ligase (New England Biolabs) in a volume of 300 µl (total of four ligations). The reaction mix was purified and retroviral insertion sites were identified via an inverse PCR protocol adapted to next-generation sequencing[45].

Immunopurification and nano-liquid chromatography (LC)–mass spectrometry (MS) analysis. Anti-BRD4 (catalog no. A301-985A100; Bethyl Laboratories) antibody (50 µg) was coupled to 100 µl AminoLink Coupling Resin (Thermo Fisher Scientific). Cell lysate samples (5 mg) were incubated with prewashed immuno-resin on a shaker for 2 h at 4 °C. Beads were washed in lysis buffer containing 0.4% octylphenoxypolyethoxyethanol and lysis buffer without detergent followed by two washing steps with 150 mM NaCl. Samples were processed by on-bead digest with endoproteinase Lys-C and glycine protease before they were reduced, alkylated and digested with trypsin.

The nano HPLC system used was an UltiMate 3000 HPLC RSLC nano system (Thermo Fisher Scientific) coupled to a Q Exactive hybrid quadrupole-Orbitrap mass spectrometer (Thermo Fisher Scientific), equipped with a Proxeon nanospray source (Thermo Fisher Scientific).

The Q Exactive mass spectrometer was operated in data-dependent mode, using a full scan (*m/z* range 350–1,650, nominal resolution of 70,000, target value 1×10^6) followed by tandem mass spectrometry (MS/MS) scans of the 12 most abundant ions. MS/MS spectra were acquired using a normalized collision energy of 30%, an isolation width of 2 and the target value was set to 5×10^4. Precursor ions selected for fragmentation (charge state 2 and higher) were put on a dynamic exclusion list for 30 s. Additionally, the underfill ratio was set to 20% resulting in an intensity threshold of 2×10^4. The peptide match and exclude isotopes features were enabled.

Generation of MTHFD1 knockout HAP1 cell lines. To generate MTHFD1 knockout mutants, guide RNAs were designed using the CRISPR Design Tool (http://tools.genome-engineering.org) and cloned into pSpCas9(BB)-2A-Puro (PX459) V2.0 (plasmid no. 62988, Addgene; gift from F. Zhang)[46]. HAP1 cells were transiently transfected with PX459 containing the gRNAs by using TurboFectin 8.0 (OriGene Technologies) according to the manufacturer's instructions. Transfected cells were under puromycin selection for 2 d; afterwards, resistant cells were at a low density for single-clone picking. Knockout clones were verified by both PCR and western blotting.

Generation of MTHFD1-NES and NLS vectors. The MTHFD1 consensus coding sequence was previously inserted into pcDNA3_N-DYK by gene synthesis (GenScript) to generate the MTHFD1 complementary plasmid (MTHFD1-wild type, pcDNA3_N-DYK-MTHFD1).

To generate the pcDNA3_N-DYK_MTHFD1-NES and pcDNA3_N-DYK_MTHFD1-NLS plasmids, the NES/NLS sequences were fused to MTHFD1-wild type through site-directed mutagenesis (Q5 Site-Directed Mutagenesis Kit, New England Biolabs) according to the user's manual.

Preparation of nuclear cell extracts for metabolomics. Nuclei were extracted by hypotonic lysis. Briefly, intact cells treated as indicated in the Results section were washed twice with cold PBS and incubated on ice for 10 min with hypotonic lysis buffer (10 mM HEPES, pH 7.9, with 1.5 mM $MgCl_2$, 10 mM KCl and protease inhibitor cocktail (cOmplete; Roche); buffer/cell volume ratio 5:1). The pellet was gently resuspended three times during incubation. Nuclei were collected by centrifugation (420*g* × 5 min) and immediately snap-frozen.

The metabolomics assay and data analysis were performed by Metabolomic Discoveries (http://www.metabolomicdiscoveries.com). Briefly, LC–quadrupole time-of-flight–MS-based non-targeted metabolite profiling was used to analyze nuclear metabolites in the range of 50–1,700 Da, with an accuracy of up to 1–2 parts per million (ppm) and a resolution of mass/Δmass = 40,000. Metabolites measured in the LC were annotated according to their accurate mass and subsequent sum formula prediction. Metabolites that were not annotated in the LC–MS analyses are listed according to their accurate mass and retention time.

Folate extraction for LC–MS/MS analysis. To quantify folates in the nuclear and cytosolic fractions, 20 million HAP1 cells per condition were washed twice with cold PBS and collected into a 50 ml Falcon tube (Corning) by centrifugation for 5 min at 280*g* and 4 °C. Cell lysis was performed on ice in the dark by incubating cell pellets with 1:5 hypotonic lysis buffer for 10 min. Nuclei were collected by centrifugation for 5 min at 420*g* and 4 °C. Supernatants (cytosolic fractions) were also collected. Both fractions were immediately snap-frozen.

For the nucleus samples, 10 µl of internal standard mixture was added to the nucleus pellet in a 1.5 ml Eppendorf tube followed by adding 145 µl of ice-cold extraction solvent (10 mg ml^{-1} ascorbic acid solution in 80% methanol, 20% water, v/v). The samples were vortexed for 10 s, then incubated on ice for 3 min and vortexed again for 10 s. After centrifugation (14,000 r.p.m., 10 min, 4 °C),

the supernatant was collected into HPLC vials. The extraction step was repeated and the combined supernatants were used for LC–MS/MS analysis.

For the cytoplasm samples, 10 µl of internal standard mixture was added to 75 µl of cytoplasm in a 1.5 ml Eppendorf tube followed by adding 215 µl of ice-cold extraction solvent (10 mg ml^{-1} ascorbic acid solution in 80% methanol, 20% water, v/v). The samples were vortexed for 10 s, then incubated on ice for 3 min and vortexed again for 10 s. After centrifugation (14,000 r.p.m., 10 min, 4 °C), the supernatant was collected into HPLC vials and used for the LC–MS/MS analysis.

LC–MS/MS analysis of folates. An ACQUITY UHPLC I-Class (Waters) coupled with a Xevo TQ-S IVD System (Waters) was used for the quantitative analysis of metabolites. The separation was conducted on an ACQUITY UPLC HSS T3, 1.8 µm, 2.1 × 100 mm column (Waters) equipped with an ACQUITY UPLC HSS T3 1.8 µM VanGuard pre-column (Waters) at 40 °C. The separation was carried out using 0.1% formic acid (v/v) in water as a mobile phase A, and 0.1% formic acid (v/v) in methanol as a mobile phase B. The gradient elution with a flow rate 0.5 ml min^{-1} was performed with a total analysis time of 10 min. The autosampler temperature was set to 4 °C. For detection purposes, the Xevo TQ-S IVD System in positive electrospray ionization mode with multiple reaction mode was employed. Quantification of all metabolites was performed using the MassLynx v.4.1 software (Waters). Seven-point linear calibration curves with internal standardization and 1/x weighting were constructed for the quantification.

Sodium formate-^{13}C sample preparation and ^{13}C tracing analysis of nucleotides by LC–MS. HAP1 wild-type and MTHFD1 knockout cells were seeded at 350,000 cells ml^{-1} in media containing 1 mM sodium formate-^{13}C (Cambridge Isotope Laboratories (CDLM-6203-0.5)) for 24 h. After incubation, RNA was extracted using the RNeasy Mini Kit (QIAGEN); 2 µg of RNA were hydrolyzed to single nucleotides (alkaline hydrolysis) with 0.3 N NaOH for 16 h at 37 °C, shaking at 300 r.p.m. and 0.3 N HCl was added to neutralize the alkaline pH. For the LC–MS analysis, 40 µl of methanol was added to 10 µl of hydrolyzed RNA solution. The samples were vortexed for 10 s, centrifuged (14,000 r.p.m., 5 min, 4 °C), and the supernatant was transferred into an HPLC vial. A Vanquish UHPLC System (Thermo Fisher Scientific) coupled with an Orbitrap Fusion Lumos Tribrid mass spectrometer (Thermo Fisher Scientific) was used for the ^{13}C tracing analysis of nucleotides. The separation was carried out on an ACQUITY UPLC BEH Amide, 1.7 µm, 2.1 × 100 mm analytical column (Waters) equipped with a VanGuard BEH C18, 2.1 × 5 mm pre-column (Waters). A gradient elution using 0.15% formic acid (v/v) in water as mobile phase A and 0.15% formic acid (v/v) in 85% acetonitrile (v/v) with 10 mM ammonium formate as mobile phase B was applied. For detection purposes, an Orbitrap Fusion Lumos Tribrid mass spectrometer in positive ionization mode was employed. Isotopologue distribution was acquired using an Orbitrap MS scan with a 500,000 resolution, scan range from 110 to 500 *m/z*, automatic gain control target of 2×10^5 and maximum injection time of 50 ms. The TraceFinder v.4.1 software (Thermo Fisher Scientific) was used to process the data.

ChIP-seq sample preparation. Three 15 cm dishes with cells at 70–80% confluency were used for one ChIP-seq experiment. Briefly, cells were cross-linked with 1% formaldehyde for 10 min at room temperature, and then quenched with 125 mM glycine for 5 min at room temperature. Then, cells were washed with cold PBS, collected in 15 ml tubes, washed again with cold PBS by centrifugation at 1,200 r.p.m. for 5 min at 4 °C and finally snap-frozen.

ChIP-seq was performed as described[47] by using BRD4 (catalog no. A301-985A100; Bethyl Laboratories) and MTHFD1 (catalog no. sc-271413; Santa Cruz Biotechnology) antibodies. In brief, cross-linked cell lysates were sonicated to shred the chromatin into 200–500 bp fragments. Fragmented chromatin was incubated overnight at 4 °C with antibodies, followed by 2 h at 4 °C with pre-blocked Dynabeads Protein G (Thermo Fisher Scientific). Beads were washed twice with low-salt solution buffer, twice with high-salt solution buffer, twice with LiCl buffer, twice with 1× Tris-EDTA buffer and finally eluted with elution buffer for 20 min at 65 °C. The elution products were treated with RNase A (Thermo Fisher Scientific) for 30 min at 37 °C, followed by proteinase K treatment at 55 °C for 1 h; then, it was incubated at 65 °C overnight to reverse the cross-links. The samples were further purified by using a PCR Purification Kit (QIAGEN).

ChIP-seq and RNA-seq data analysis. Next-generation sequencing libraries were sequenced by the Biomedical Sequencing Facility at CeMM using the HiSeq 3000/4000 platform and the 50-bp single-end configuration. For ChIP-seq, reads containing adapters were trimmed using Skewer[48] and aligned to the hg19/GRCh37 assembly of the human genome using bowtie2 v.2.2.9 (ref. [49]) with the '--very-sensitive' parameter; duplicate reads were marked and removed with sambamba v.0.6.7. Library quality was assessed with the phantompeakqualtools scripts[50]. We used HOMER findPeaks v.4.8[51] to call peaks on both replicates with matched IgG controls as background. This was done in 'in factor' mode for BRD4 and in 'histone' mode for MTHFD1. We used the Genomic Regions Enrichment of Annotations Tool (GREAT) v.3.0.0[52] to assign regions to putative regulated genes with default parameters and to retrieve enriched gene functions from BRD4- or MTHFD1-bound regions. For visualization, we generated genome browser tracks with deepTools2.0 (ref. [53]) using reads per bin scaled to 1× genome coverage normalization, which were also input to generate visualizations of ChIP-seq signal in peaks either for each peak or in aggregate. This was done for each sample individually and for merged replicates. DiffBind v.2.8.0[54] was used to detect differential binding of BRD4 or MTHFD1 in a consensus set of bound regions by the two factors, for MTHFD1 knockout or dBET6-treated samples against the respective controls. Regions with an absolute $\log_2$ fold change >1 and an FDR-adjusted $P < 0.1$ were used to display ChIP-seq intensity values using the estimated concentration values from DiffBind. Total differences between ChIP-seq levels in these regions between conditions were tested with a Mann–Whitney *U*-test. For RNA-seq data, we used reads per kilobase of transcript per million mapped reads values as estimated by the Cufflinks software suite v.2.1.1 [55] and used the limma removeBatchEffect function to integrate datasets produced in different batches with default parameters. Genes associated with differentially bound sites by BRD4 or MTHFD1 as retrieved from GREAT were used to display the distributions of $\log_2$ fold changes of expression as estimated by the Cufflinks links for RNA-seq data. Overlap between bound and differentially expressed genes was tested with a Fisher's exact test and *P* values were corrected with the FDR method. All epigenomic data (Gene Expression Omnibus (GEO) accession no. GSE105786) and the data analysis code (https://github.com/epigen/mthfd1) are available.

Mouse xenograft studies. Mouse xenograft studies were performed as described previously[27]; 2×10^6 A549 cells, diluted 1:1 in Matrigel, were transplanted subcutaneously into NOD *scid* gamma mice. Treatment (30 mg kg^{-1} (*S*)-JQ1 by intraperitoneal injection five times per week and 25 mg kg^{-1} MTX via intraperitoneal injection twice weekly) was started when tumors were established, 19 d post-transplantation. Tumor volumes were evaluated twice a week by measuring two perpendicular diameters with calipers. Tumor volume was calculated using the following equation: (width × width × length)/2. Treatment was performed according to an animal license protocol approved by the Bundesministerium für Wissenschaft und Forschung (no. BMWF-66.009/0280-II/3b/2012). At day 43, mice were killed and tumors were excised and weighted.

Supplementary note. The Supplementary Note contains the following supplementary methods:

immunofluorescence, metaphase spread and live cell imaging; cell cycle assay; RNA extraction and RT–PCR; cell sorting; FISH assay; AlphaLISA assay; preparation of nuclear cell extracts for proteomics; peptide microarrays; MS data analysis (proteomics); molecular modeling; chromatin purification and LC–MS/MS analysis; MS data analysis (chromatin fraction); GO term enrichment analysis (MTHFD1 pull-down on chromatin); in vitro metabolomics and folate extraction for LC–MS/MS analysis; metabolite set enrichment analysis.

Statistics. The statistical tests used are described in the respective figure legends and methods sections.

The following figure panels are representative of experiments repeated the following number of times: Fig. 1c—triplicate; Fig. 1d—triplicate; Fig. 1e—duplicate; Fig. 2b—duplicate; Fig. 2c—triplicate; Fig. 2d—triplicate; Fig. 2e—duplicate; Fig. 2f—duplicate; Fig. 3a—triplicate; Fig. 4b—duplicate.

Reporting Summary. Further information on research design is available in the Nature Research Reporting Summary linked to this article.

Data availability

Next-generation sequencing data have been deposited with the National Center for Biotechnology Information GEO (accession no. GSE105786). Proteomics data have been deposited with the PRIDE Archive (accession nos. PXD012715 and PXD013090).

References

43. Bürckstümmer, T. et al. A reversible gene trap collection empowers haploid genetics in human cells. *Nat. Methods* **10**, 965–971 (2013).
44. Krzywinski, M. et al. Circos: an information aesthetic for comparative genomics. *Genome Res.* **19**, 1639–1645 (2009).
45. Carette, J. E. et al. Global gene disruption in human cells to assign genes to phenotypes by deep sequencing. *Nat. Biotechnol.* **29**, 542–546 (2011).
46. Ran, F. A. et al. Genome engineering using the CRISPR-Cas9 system. *Nat. Protoc.* **8**, 2281–2308 (2013).
47. Kim, T. H. et al. A high-resolution map of active promoters in the human genome. *Nature* **436**, 876–880 (2005).
48. Jiang, H., Lei, R., Ding, S. W. & Zhu, S. Skewer: a fast and accurate adapter trimmer for next-generation sequencing paired-end reads. *BMC Bioinformatics* **15**, 182 (2014).
49. Langmead, B. & Salzberg, S. L. Fast gapped-read alignment with Bowtie 2. *Nat. Methods* **9**, 357–359 (2012).

50. Landt, S. G. et al. ChIP-seq guidelines and practices of the ENCODE and modENCODE consortia. *Genome Res.* **22**, 1813–1831 (2012).
51. Heinz, S. et al. Simple combinations of lineage-determining transcription factors prime *cis*-regulatory elements required for macrophage and B cell identities. *Mol. Cell* **38**, 576–589 (2010).
52. McLean, C. Y. et al. GREAT improves functional interpretation of *cis*-regulatory regions. *Nat. Biotechnol.* **28**, 495–501 (2010).
53. Ramírez, F. et al. deepTools2: a next generation web server for deep-sequencing data analysis. *Nucleic Acids Res.* **44**, W160–W165 (2016).
54. Ross-Innes, C. S. et al. Differential oestrogen receptor binding is associated with clinical outcome in breast cancer. *Nature* **481**, 389–393 (2012).
55. Trapnell, C. et al. Transcript assembly and quantification by RNA-Seq reveals unannotated transcripts and isoform switching during cell differentiation. *Nat. Biotechnol.* **28**, 511–515 (2010).

nature research

Corresponding author(s): Stefan Kubicek

Reporting Summary

Nature Research wishes to improve the reproducibility of the work that we publish. This form provides structure for consistency and transparency in reporting. For further information on Nature Research policies, see Authors & Referees and the Editorial Policy Checklist.

Statistical parameters

When statistical analyses are reported, confirm that the following items are present in the relevant location (e.g. figure legend, table legend, main text, or Methods section).

n/a	Confirmed	
☐	☒	The exact sample size (*n*) for each experimental group/condition, given as a discrete number and unit of measurement
☐	☒	An indication of whether measurements were taken from distinct samples or whether the same sample was measured repeatedly
☐	☒	The statistical test(s) used AND whether they are one- or two-sided *Only common tests should be described solely by name; describe more complex techniques in the Methods section.*
☐	☒	A description of all covariates tested
☐	☒	A description of any assumptions or corrections, such as tests of normality and adjustment for multiple comparisons
☐	☒	A full description of the statistics including central tendency (e.g. means) or other basic estimates (e.g. regression coefficient) AND variation (e.g. standard deviation) or associated estimates of uncertainty (e.g. confidence intervals)
☐	☒	For null hypothesis testing, the test statistic (e.g. *F*, *t*, *r*) with confidence intervals, effect sizes, degrees of freedom and *P* value noted *Give P values as exact values whenever suitable.*
☒	☐	For Bayesian analysis, information on the choice of priors and Markov chain Monte Carlo settings
☒	☐	For hierarchical and complex designs, identification of the appropriate level for tests and full reporting of outcomes
☐	☒	Estimates of effect sizes (e.g. Cohen's *d*, Pearson's *r*), indicating how they were calculated
☐	☒	Clearly defined error bars *State explicitly what error bars represent (e.g. SD, SE, CI)*

Our web collection on statistics for biologists may be useful.

Software and code

Policy information about availability of computer code

Data collection	Raw sequencing data from gene-trap screens were aligned to human reference genome hg19 (UCSC hg19 build) using bowtie2 (version 2.2.4) with default parameters. Duplicate reads were marked and discarded with Picard (version 1.111). Insertions in close proximity (1 or 2 base pairs distance from each other) were removed to avoid inclusion of insertions due to mapping errors. Insertions were annotated with gene build GRCh37.p13 (ENSEMBL 75 - release February 2014) using bedtools (version 2.10.1). For ChIP-seq, reads containing adapters were trimmed using Skewer 51 and aligned to the hg19/GRCh37 assembly of the Human genome using Bowtie2 52 with the "--very-sensitive" parameter and duplicate reads were marked and removed with sambamba.
Data analysis	For gene trap screens, insertion plots were drawn with R statistics software and circos plots were produced using circos Circos. For ChIP-seq analysis, library quality was assessed with the phantomPeakQualtools scripts . We used HOMER findPeaks to call peaks on both replicates with matched IgG controls as background. We used GREAT to assign regions to putative regulated genes with default parameters and to retrieve enriched gene functions from BRD4 or MTHFD1 bound regions. For visualization, we generated genome browser tracks with deeptools2 using RPGC normalization (reads per bin scaled to 1X genome coverage) which were also input to generate visualizations of ChIP-seq signal in peaks either for each peak or in aggregate. TDiffBind57 was used to detect differential binding of BRD4 or MTHFD1 . For RNA-seq data, we used RPKM values as estimated by the Cufflinks software suite. For BRD4 interactome peptide identification, the RAW-files were loaded into Proteome Discoverer (version 1.4.0.288, Thermo Scientific). All hereby created MS/MS spectra were searched using Mascot 2.2.07 (Matrix Science, London, UK) against the human swissprot protein sequence database. Additional data processing of the triplicate runs including label-free quantification was performed in MaxQuant using the Andromeda search engine applying the same search parameters as for Mascot database search. For subsequent statistical analysis

Perseus software platform was used to create volcano plots, heat maps and hierarchical clustering.
For the MTHFD1 IP-MS experiment, acquired raw data files were processed using the Proteome Discoverer 2.2.0.388 platform, utilizing the database search engine Sequest HT. Percolator V3.0 was used to remove false positives with a false discovery rate (FDR) of 1% on peptide and protein level under strict conditions. Searches were performed with full tryptic digestion against the human SwissProt database v2017.07 (20,158 sequences appended with known contaminants) with up to one miscleavage site.
The functional enrichment analysis of MTHFD1 interacting proteins was performed via programmatic access to Enrichr (http://amp.pharm.mssm.edu/Enrichr/) using 'GO_Biological_Process_2018' library. Redundant GO terms with semantic similarity score > 0.4 were filtered out via Revigo (http://revigo.irb.hr). Metabolite set enrichment analysis (MSEA) was performed using the online tool MetaboAnalyst (http://www.metaboanalyst.ca/).
Quantification of all metabolites was performed using MassLynx V4.1 software from Waters. TraceFinder software (Thermo) was employed for the data processing of isotope labelling experiments

For manuscripts utilizing custom algorithms or software that are central to the research but not yet described in published literature, software must be made available to editors/reviewers upon request. We strongly encourage code deposition in a community repository (e.g. GitHub). See the Nature Research guidelines for submitting code & software for further information.

Data

Policy information about availability of data

All manuscripts must include a data availability statement. This statement should provide the following information, where applicable:

- Accession codes, unique identifiers, or web links for publicly available datasets
- A list of figures that have associated raw data
- A description of any restrictions on data availability

Next generation sequencing data have been deposited to NCBI GEO (accession GSE105786), proteomics data have been deposited to PRIDE (accessions PXD012715, PXD013090).

Field-specific reporting

Please select the best fit for your research. If you are not sure, read the appropriate sections before making your selection.

☒ Life sciences ☐ Behavioural & social sciences ☐ Ecological, evolutionary & environmental sciences

For a reference copy of the document with all sections, see nature.com/authors/policies/ReportingSummary-flat.pdf

Life sciences study design

All studies must disclose on these points even when the disclosure is negative.

Sample size	All experiments were performed in independent biological replicates, replicate numbers are indicated in the manuscript. Sample sizes were chosen method-specifically. For animal experiments, sample sizes (n=10 per group) were chosen based on anticipated effect sizes, taking into consideration type 1 error rate and study power.
Data exclusions	No data were excluded.
Replication	All replication data are included and confirm the original findings.
Randomization	Different biological replicates were performed on separated days, with samples collected from separated cell culture batches and processed by different members of the group. For mouse xenograft studies, animals were randomly assigned to the four different treatment groups.
Blinding	Due to the largely biochemical nature of the study, samples were not blinded. In order to minimise bias, each sample was identified with a number instead of with its specific experimental condition (e.g. “1” instead than “untreated”).

Reporting for specific materials, systems and methods

Materials & experimental systems

n/a	Involved in the study
☒	☐ Unique biological materials
☐	☒ Antibodies
☐	☒ Eukaryotic cell lines
☒	☐ Palaeontology
☐	☒ Animals and other organisms
☒	☐ Human research participants

Methods

n/a	Involved in the study
☐	☒ ChIP-seq
☐	☒ Flow cytometry
☒	☐ MRI-based neuroimaging

Antibodies

Antibodies used

The following antibodies were used for Western blotting: BRD4 (ab128874, 1:1000, Abcam), Actin (ab16039, 1:1000, Abcam), MTHFD1 (ab70203, Abcam; H120, Santa Cruz; A8, Santa Cruz. All used at 1:1000), MTHFD1L (ab229708, 1:1000, Abcam), MTHFD2 (ab151447, 1:1000, Abcam), GFP (G10362, 1:1000, Life Technology), RCC1 (C-20, 1:1000, Santa Cruz), -Tubulin (T-4026, 1:1000, Sigma), SHMT1 (ab186130, 1:1000, Abcam), SHMT2 (ab180786, 1:1000, Abcam), DHFR (ab49881, 1:1000, abcam), Lamin-B (ab16048, 1:1000, Abcam), VDAC-1 (ab15895, 1:1000, Abcam) and H2B (ab156197, 1:1000, Abcam) and detected by HRP (horseradish peroxidase) conjugated donkey anti-rabbit IgG antibody (ab16284, 1:5000, Abcam) or donkey anti-mouse IgG antibody (Pierce).
The following antibodies were used for ChIP-Seq: BRD4 (Bethyl Laboratories, Inc.) and MTHFD1 (sc-271413, Santa Cruz)
IP for MS: BRD4 (Bethyl Laboratories, Inc.), MTHFD1 A8 (Santa Cruz).

Validation

All antibodies have been described and validated previously. For key antibodies we use knock-down/degradation of the target to validate them, these data are included in our manuscript.
BRD4 ab128874, KO tested (https://www.abcam.com/brd4-antibody-epr51502-ab128874.html)
Actin ab16039 has 42 references (https://www.abcam.com/beta-actin-antibody-ab16039.html)
SHMT1 ab186130 has been validated by Abcam by WB and has 1 reference (https://www.abcam.com/shmt1-antibody-ab186130.html)
SHMT2 ab180786 has been validated by Abcam by WB and has 2 references (https://www.abcam.com/shmt2shmt-antibody-c-terminal-ab180786-references.html#top-218)
DHFR ab49881 has been validated by several Abcam customers and has 6 references (https://www.abcam.com/dihydrofolate-reductase-dhfr-antibody-ab49881.html?productWallTab=Abreviews)
MTHFD1L ab229708 has been validated by Abcam by WB
MTHFD2 ab151447 has been validated by 3 Abcam customers and has 2 references (https://www.abcam.com/mthfd2-antibody-ab151447.html)
GFP G10362 has 99 references (https://www.thermofisher.com/antibody/product/GFP-Tag-Antibody-Monoclonal/G10362)
RCC1 C-20 has been used in 7 publications (https://www.scbt.com/scbt/product/rcc1-antibody-c-20)
Tubulin T-4026 has been used in 580 publications (https://www.sigmaaldrich.com/catalog/product/sigma/t4026?lang=es&region=ES&gclid=Cj0KCQjw7YblBRDFARIsAKkK-dJFFhYcSo9Rpb_kQUU1K4V7UIK5k47p-5JgJQi3jpurGArrbC1Kpu4aAllEEALw_wcB)
Lamin-B ab16048 has been KO validated by Abcam and cited in 442 publication (https://www.abcam.com/lamin-b1-antibody-nuclear-envelope-marker-ab16048.html)
VDAC-1 ab15895 has been validated by 26 Abcam customers and cited in 175 publications (https://www.abcam.com/vdac1-porin-antibody-mitochondrial-loading-control-ab15895.html)
BRD4 Bethyl Laboratories has been cited in 31 publications (https://www.bethyl.com/product/A301-985A100/BRD4+Antibody)

All the used MTHFD1 Antibodies have been validated with our MTHFD1 KO cell lines

Eukaryotic cell lines

Policy information about cell lines

Cell line source(s)

HAP1, Horizon Genomics
KBM7, Horizon Genomics
K-562, ATCC
MV4-11, ATCC
HeLa, ATCC
MOLM-13, ATCC
NOMO-1, ATCC
A459, ATCC
HEK293, ATCC

Authentication

Cell lines were used as provided by vendors without further authentication.

Mycoplasma contamination

All cell lines were tested and confirmed mycoplasma negative

Commonly misidentified lines
(See ICLAC register)

none of the used cell lines is a commonly misidentified line according to the ICLAC register

Animals and other organisms

Policy information about studies involving animals; ARRIVE guidelines recommended for reporting animal research

Laboratory animals	For the xenograft studies, male NOD SCID gamma mice at 3/4 weeks age were used.
Wild animals	No wild animals were used.
Field-collected samples	No field-collected samples were used .

ChIP-seq

Data deposition

☒ Confirm that both raw and final processed data have been deposited in a public database such as GEO.

☐ Confirm that you have deposited or provided access to graph files (e.g. BED files) for the called peaks.

Data access links *May remain private before publication.*	We make all epigenomics data available at GEO accession GSE105786
Files in database submission	128 samples deposited
Genome browser session (e.g. UCSC)	http://genome.ucsc.edu/cgi-bin/hgTracks?db=hg19&hubUrl=http://biomedical-sequencing.at/bocklab/arendeiro/mthfd1/hub.txt

Methodology

Replicates	ChIP-Seq studies were performed in duplicate.
Sequencing depth	ChIP-seq libraries were sequenced by the Biomedical Sequencing Facility at CeMM using the Illumina HiSeq3000/4000 platform and the 50-bp single-end configuration.
Antibodies	Included in the methods section
Peak calling parameters	Included in the ChIP-seq data analysis section
Data quality	Included in the ChIP-seq data analysis section
Software	Included in the ChIP-seq data analysis section

Flow Cytometry

Plots

Confirm that:

☒ The axis labels state the marker and fluorochrome used (e.g. CD4-FITC).

☒ The axis scales are clearly visible. Include numbers along axes only for bottom left plot of group (a 'group' is an analysis of identical markers).

☐ All plots are contour plots with outliers or pseudocolor plots.

☒ A numerical value for number of cells or percentage (with statistics) is provided.

Methodology

Sample preparation	n/a
Instrument	BD FACSCalibur Flow Cytometer and FACSAria (BD Biosciences)
Software	SUMMIT
Cell population abundance	Included in the manuscript.
Gating strategy	Included in the manuscript.

☐ Tick this box to confirm that a figure exemplifying the gating strategy is provided in the Supplementary Information.